Honeycomb Constructs in the La–Ni Intermetallics: Controlling Dimensionality via p -Element Substitution

Vitalii Shtender, Volodymyr Smetana, Jean-Claude Crivello, Łukasz Gondek, Janusz Przewoźnik, Anja-Verena Mudring, Martin Sahlberg

Honeycomb constructs in the La-Ni intermetallics: Controlling dimensionality via *p*-element substitution

Vitalii Shtender[1], Volodymyr Smetana[2], Jean-Claude Crivello[3], Łukasz Gondek[4], Janusz Przewoźnik[4], Anja-Verena Mudring[2], Martin Sahlberg[1]

[1]*Department of Chemistry – Ångström Laboratory, Uppsala University, Box 538, 751 21, Uppsala, Sweden*

[2]*Department of Materials and Environmental Chemistry, Stockholm University, Svante Arrhenius väg 16c, 10691 Stockholm, Sweden*

[3]*Univ Paris Est Creteil, CNRS, ICMPE, UMR7182, 2 rue Henri Dunant, 94320 Thiais, France*

[4]*AGH University of Science and Technology, Faculty of Physics and Applied Computer Science, Mickiewicza 30, 30-059, Krakow, Poland*

Abstract

The new ternary compounds $La_{15}Ni_{13}Bi_5$ and $La_9Ni_8Sn_5$ were obtained by arc melting under argon from appropriate amounts of the elements and subsequent annealing at 800 °C for two weeks. Single crystal X-ray diffraction reveals that they represent two new structure types: $La_{15}Ni_{13}Bi_5$ crystallizes in the hexagonal space group $P\bar{6}2m$ (*hP*33, a = 14.995(3), c = 4.3421(10) Å, V = 845.5(4) Å^3, Z = 1) and $La_9Ni_8Sn_5$ in $P6_3/m$ (*hP*88, a = 23.870(15), c = 4.433(3) Å, V = 2187(3) Å^3, Z = 4). The crystal structures of both compounds are characterized by hexagonal honeycomb-based motifs formed by Ni and Sn extending along the *c* axis. The building motif with its three-blade wind turbine shape reminds of the organic molecule triptycene and is unprecedented in extended solids. First-principles calculations have been performed in order to analyze the electronic structure and provide insight into chemical bonding. They reveal significant electron transfer from La to Ni and the respective *p*-element, which supports the formation of the polyanionic Sn-p-element network. DFT calculations suggest paramagnetic-like behavior for both compounds, which was confirmed by magnetic measurements.

1. Introduction

Bismuth and tin based intermetallic compounds are interesting for many technologies and high-tech applications. They own many unique and desirable properties for optoelectronic, solders, fusible alloys, substitutes of lead, thermoelectric, superconductors, and electronic device applications.[1-3] Superconductivity has been observed in many *p*-elements such as Sn and their binary intermetallic compounds like in the La-Sn system.[4-6] Nb_3Sn shows excellent superconducting performance at lower temperatures and under high magnetic fields.[7] Pd_3Bi has been applied in catalysis,[8] bismuth tellurides found their application as superconductors, advanced thermoelectric materials, in mobile refrigerators or infrared detectors.[9] La-Ni alloys feature enhanced hydrogen sorption, and through the addition of certain *p* elements their mechanical resistance is improved, as in $LaNi_5Sn$, although sacrificing capacity.[10-11]

Interestingly, the ternary La-Ni-Sn system has been only partially investigated resulting in a preliminary phase diagram at 400 °C.[12] So far, eight ternary compounds have been confirmed: $LaNi_5Sn$ ($CeNi_5Sn$ type),[13] $LaNi_4Sn_2$ (KAu_4Sn_2 type),[14] $LaNi_2Sn_2$ ($CaBe_2Ge_2$ type),[15] $La_3Ni_2Sn_6$ = $LaNi_{0.7}Sn_2$ ($CeNiSi_2$ type),[16] $La_3Ni_2Sn_7$ ($La_3Co_2Sn_7$ type),[17] $La_3Ni_8Sn_{16}$ = $La_{4.87}Ni_{12}Sn_{24}$ ($Gd_4(Gd_{0.5}Sn_{0.5})Ni_{12}Sn_{24}$ type),[18] LaNiSn (TiNiSi type),[19] $La_5Ni_{24}Sn$ = $LaNi_{4.8}Sn_{0.2}$ (essentially a solid solution based on $LaNi_5$) ($CaCu_5$ type).[20] $LaNiSn_3$ has been mentioned but no crystal structure has ever been reported.[21] LaNiSn shows polymorphism under pressure switching from the TiNiSi type to the ZrNiAl type.[22]. All ternary compounds in this system (up to date) are La-poor, reaching a maximum of 33.3 at.% of La.[21] The related La-Ni-Bi system has been even more poorly investigated with only three ternary compounds reported so far: La_2NiBi (La_2NiSb-type),[23] $LaNi_{2-x}Bi_2$ ($CaBe_2Ge_2$-type for x= 0.5 and $CuHfSi_2$-type for x= 1.16)[24-25] and $La_3Ni_3Bi_4$ ($Y_3Au_3Sb_4$-type)[26] and no phase equilibria has been established.

This prompted us to close the knowledge gap and re-investigate the ternary La-Ni-*X* systems with *X* = Sn, Bi. During these explorations, two new compounds were discovered with interesting structural features, namely hexagonal honeycomb motifs extending along the main axis, $La_{15}Ni_{13}Bi_5$ and $La_9Ni_8Sn_5$. These motifs remind of the three-blade wind turbine shape of triptycene and are unprecedented in extended solids. In the present work, we report on their crystal- and electronic structures, analyze the chemical bonding and discuss relationships with other intermetallics.

2. Methodology

2.1 Experimental part

La/M/Ni (*M* = Bi and Sn) alloys (1g each) with the molar ratios of the elements 15:13:5 and 9:8:5, respectively, were synthesized by arc-melting of high purity La (99.9%), Ni (99.99%), Bi (99.9%) and Sn (99.999) from Alfa Aesar. An excess of Bi (1 wt.%) was used to compensate for losses during the melting. Oxygen contamination was minimized by flushing the furnace five times with Ar and by melting a Ti getter before melting the sample. The sample ingots were turned over and re-melted three times to promote homogeneity. The ingots then were wrapped in Ta-foil, placed in a quartz tube and sealed under a vacuum for later annealing at 800 °C for two weeks. Subsequently, samples were quenched in cold water.

An alternative method has also been used to get crystals of better quality. According to the binary La-Ni phase diagram, alloys in the region of 50-80 at.% of La exhibit relatively low melting points below 700 °C. Therefore, $La_{15}Ni_{13}$ and La_9Ni_8 ligatures were prepared by arc melting, crushed and mixed with appropriate amounts Bi and Sn. The mixtures were loaded into Ta tubes and sealed under an Ar atmosphere and subsequently placed in stainless steel tubes to protect from oxidation. The samples were slowly heated (10h) up to 1000 °C, kept for 1h and cooled at 3 °C/h down to 500 °C. For cooling to room temperature, the furnace was switched off.

Intensity data sets for powder X-ray diffraction (PXRD) were recorded at room temperature using a Bruker D8 X-ray diffractometer with a Lynx-eye position sensitive detector and Cu-Kα radiation on a zero-background single crystal Si sample holder. Phase analyses (**Figure S1** in Supporting Information (SI)) using the Rietveld method of the powder X-ray data were performed using TOPAS v6 software.[27]

Single-crystal X-ray diffraction (SXRD) data were collected at 293 K on a Bruker D8 Venture diffractometer (Bruker, USA; Photon 100 CMOS detector, IμS microfocus source: Mo K_α radiation, λ = 0.71073 Å, 2 –5). Intensity data sets of reflections and scaling were integrated within the APEX3 software package by using SAINT.[28] Absorption corrections were conducted with SADABS[29] and crystal structure solutions with SHELXT.[30] For subsequent difference Fourier analyses and least-squares refinements, SHELXL-2013[31] was used. The mixed Sn1/Ni1 position in $La_9Ni_8Sn_5$ has initially been refined with independent occupation resulting in a 1:2 ratio within 1 sigma. Therefore, the occupations of the Sn and Ni components have been restricted to 1/3 and 2/3. Such occupation matches well with the neighboring positionally disordered La2-La3-La4

positions explaining somewhat higher ADPs. The experimental details of the crystal structure determination and refinement as well as the atomic coordinates have been collected in **Tables 1** and **2**. Studied crystals were well stable in air (checked after 1 month) but the alloys in general could slightly be affected by hydrolysis (a minor amount of $La(OH)_3$ was identified from the PXRD).

The microstructure was evaluated with a Zeiss Merlin SEM equipped with a secondary electron (SE) detector and an energy-dispersive X-ray (EDX) spectrometer. The samples for electron microscopy analysis were prepared by standard metallographic techniques through grinding with SiC paper. For the final polishing, a mixture of SiO_2 and H_2O was used. SEM images together with EDX compositions are presented in **Figure S2**.

Magnetic measurements were conducted using a Physical Property Measurement System (PPMS, Quantum Design, USA). Vibrating Sample Magnetometer (VSM) options were utilized to measure zero-field cooled (ZFC) and field-cooled (FC) magnetization between 2 and 300 K in static fields (DC) up to 7 T. Isothermal magnetization was acquired in applied fields up to 7 T. Polycrystalline samples (30-65 mg) were filled into polypropylene (PP) capsules, which were mounted into a brass sample holder.

2.2 First Principles calculations

The electronic structure of $La_{15}Ni_{13}Bi_5$ and $La_9Ni_8Sn_5$ were calculated in the DFT framework in a pseudo-potential approach in the projector augmented-wave (PAW) method with collinear spin polarization using the VASP package,[32-33] but without spin-orbital coupling. The generalized gradient approximation (GGA) described with the PBE function[34] was used with a cutoff energy of 600 eV, within a high k-mesh density (about 200 points in the irreducible Brillouin zone). Preserving the original crystal symmetry, each structure was fully relaxed by several relaxation schemes (volume, cell shape as the *c*/*a* ratio, and atomic positions).

Based on the experimental observation, the crystal structures of $La_{15}Ni_{13}Bi_5$ and $La_9Ni_8Sn_5$ were described using the hexagonal cells (see 3.1 for crystallographic details). Whereas $La_{15}Ni_{13}Bi_5$ was considered in the ordered structure (33 atoms/cell), the $La_9Ni_8Sn_5$ was studied within a disordered description. To deal with the (2/3, 1/3) occupation by (Ni, Sn) on the 6*g* (*x*= 0.01090, *x*, *z*= 1/4) site for $La_9Ni_8Sn_5$, several "locally ordered" supercells representing a wide range of possibilities have been considered (2x2x1 cell leading to 88 atoms/cell). After relaxation, the most

stable arrangement corresponds to the one that maximizes the number of Ni pairs. Therefore, this was used for further discussion.

A careful relaxation was performed so that the convergence of Hellmann-Feynman forces was better than 0.05 meV $Å^{-1}$. Then, the phonon calculations are carried out in the harmonic approximation for $La_9Ni_8Sn_5$ from the supercell approach (1x1x2) with the finite displacement method[35] using the Phonopy code.[36] The Electron Localization Function (ELF),[37-39] which defines a region of space that can be associated with an electron pair, was computed for the valence electrons and is represented using the VESTA package.[40] Charge transfers are computed using Bader's prescription.[41]

Table1. Crystallographic data and experimental details of the structure determination for $La_{15}Ni_{13}Bi_5$ and $La_9Ni_8Sn_5$. Experiments were carried out at 296 K with Mo *K*α radiation.

Empirical formula	$La_{15}Ni_{13}Bi_5$	$La_9Ni_8Sn_5$
CSD	2241021	2241022
Composition in at.% from SCXRD	$La_{45.46}Ni_{39.39}Bi_{15.15}$	$La_{40.91}Ni_{36.36}Sn_{22.73}$
Composition at.% from EDX	$La_{45.9(4)}Ni_{38.7(4)}Bi_{15.4(1)}$	$La_{42.3(9)}Ni_{35.9(8)}Sn_{21.8(4)}$
Structure type	own	own
Formula weight, Mr (g/mol)	3891.78	2313.32
Space group (No.)	$P\bar{6}2m$ (189)	$P6_3/m$ (176)
Pearson symbol, *Z*	*hP*33, 1	*hP*88, 4
a, Å	14.995(3)	23.870(15)
c, Å	4.342(1)	4.433(3)
V, $Å^3$	845.5(4)	2187(3)
Flack parameter	0.058(19)	–
Calculated density, ρ ($g \cdot cm^{-3}$)	7.64	7.03
Absorption coefficient, μ (mm^{-1})	51.38	29.39
Theta range for data collection (°)	1.568 – 27.494	0.985 – 25.469
F(000)	1634	3948
Range in *h k l*	$-19 \le h \le 19$, $-19 \le k \le 19$, $-5 \le l \le 5$	$-28 \le h \le 28$, $-26 \le k \le 26$, $-5 \le l \le 5$
Total No. of reflections	10252	10649
No. of independent reflections	773 (R_{eq} = 0.0411)	1418 (R_{eq} = 0.0715)
Parameters	42	100
Goodness-of-fit on F^2	1.262	1.273
Final *R* indices [$I > 2\sigma(I)$]	R_1 = 0.0223; wR_2 = 0.0583	R_1 = 0.0616; wR_2 = 0.1244
R indices (all data)	R_1 = 0.0223; wR_2 = 0.0583	R_1 = 0.0768; wR_2 = 0.1293

Extinction coefficient	0.00062(12)	0.00007(2)
$\Delta\rho_{max/min}$ ($e \cdot Å^{-3}$)	2.231/-1.874	3.696/-2.796

Table 2. Atomic coordinates and equivalent isotropic displacement parameters for $La_{15}Ni_{13}Bi_5$ and $La_9Ni_8Sn_5$.

Atom	Site	*x*	*y*	*z*	SOF	U_{eq}*100 (Å^2)
			$La_{15}Ni_{13}Bi_5$			
La1	6*k*	0.85727(10)	0.39297(9)	½	1	1.01(3)
La2	6*j*	0.86107(10)	0.61853(11)	0	1	1.10(3)
La3	3*g*	0.15591(13)	0	½	1	1.02(4)
Ni1	3*g*	0.7725(3)	0	½	1	1.55(10)
Ni2	3*g*	0.6120(3)	0	½	1	1.88(10)
Ni3	3*f*	0.8447(3)	0	0	1	1.38(9)
Ni4	3*f*	0.5291(3)	0	0	1	1.32(9)
Ni5	1*a*	0	0	0	1	1.44(17)
Bi1	3*f*	0.34021(8)	0	0	1	0.96(3)
Bi2	2*c*	⅔	⅓	0	1	0.98(3)
			$La_9Ni_8Sn_5$			
La1	6*h*	0.03119(10)	0.41743(10)	¼	1	1.80(5)
La2	6*h*	0.10878(10)	0.59537(10)	¼	1	1.81(5)
La3	6*h*	0.19299(10)	0.43421(10)	¼	1	1.80(5)
La4	6*h*	0.26465(10)	0.29701(10)	¼	1	1.97(5)
La5	6*h*	0.57044(10)	0.25505(10)	¼	1	1.89(5)
La6	6*h*	0.27278(11)	0.14851(12)	¼	1	3.05(6)
Sn1/Ni1	6*h*	0.0107(2)	0.1907(2)	¼	0.333/0.667	4.29(12)
Sn2	6*h*	0.41358(12)	0.12645(12)	¼	1	1.97(6)
Sn3	6*h*	0.51642(11)	0.36453(11)	¼	1	1.52(6)
Sn4	6*h*	0.0635(3)	0.1171(3)	¼	0.333	0.61(9)
Sn5	6*h*	0.1040(3)	0.1117(3)	¼	0.333	0.61(9)
Sn6	6*h*	0.1192(3)	0.1620(3)	¼	0.333	0.61(9)
Ni2	6*h*	0.0213(7)	0.0333(6)	¼	0.333	1.9(3)
Ni3	6*h*	0.0693(2)	0.3156(2)	¼	1	2.25(11)
Ni4	6*h*	0.2236(2)	0.5758(2)	¼	1	2.39(11)
Ni5	6*h*	0.3818(2)	0.2882(2)	¼	1	1.99(11)
Ni6	6*h*	0.5290(2)	0.0302(2)	¼	1	2.20(11)
Ni7	2*c*	⅓	⅔	¼	1	2.8(2)

3. Results and discussion

3.1 Crystal structure peculiarities

$La_{15}Ni_{13}Bi_5$ crystallizes in the hexagonal space group $P\bar{6}2m$ [*hP*33, a = 14.995(3), c = 4.342(1) Å, V = 845.5(4) Å^3, Z = 1], while $La_9Ni_8Sn_5$ in $P6_3/m$ [*hP*88, a = 23.870(15), c = 4.433(3) Å, V = 2187(3) Å^3, Z = 4]. Both compounds represent their own structure types, though exhibiting plenty of similar structural motifs. For $La_{15}Ni_{13}Bi_5$ a fully ordered structure is observed, while $La_9Ni_8Sn_5$ exhibits complex positional and occupational disorder.

The crystal structure of $La_{15}Ni_{13}Bi_5$ is characterized by pseudo-1D motifs of Ni encapsulated in La/Bi tunnels. The latter are composed of two types of fused Bi@La$_x$ polyhedra, *i.e.* alternating tricapped Bi@La$_9$ and bicapped Bi@La$_8$ trigonal prisms (**Figure 1** and S5). The tricapped prisms are regular, while the bicapped also include a (smaller) Ni atom in the Bi coordination sphere at a reasonable interatomic distance, *i.e.* (Bi@La$_8$Ni), leading to significant distortion of the central trigonal prism. Although there may be non-negligible interactions, we consider the Ni formations in the structure independently for structural clarity. The Ni atoms form a stick extending along the *c* axis (**Figure 2**). The single building unit of the stick bears a structural analogy to organic aromatic molecules like triptycene that are reminiscent of a three-blade wind turbine. To the best of our knowledge, such a structural motif has never been reported in extended solids. Each turbine blade consists of one full row of fused Ni$_6$ hexagons, while the second (central) is missing its vertices (Figure S3). Instead, two lower Ni atoms are shared with two identical blades. The Ni-Ni distances within the hexagons are 2.414–2.498(9) Å while those connecting the blades are a little shorter, 2.334(8) Å, all below or around the sum of the covalent radii.[42] The outer Ni vertices connect with Bi atoms from the irregular prisms ($d_{Ni\text{-}Bi}$ = 2.836(8) Å). All other Ni positions have a coordination number of 9 and a coordination sphere of a practically ideal tricapped trigonal prism Ni@Ni$_3$La$_6$ (Figure S4). La$_6$ prisms lie normal to the blade plane fully wrapping the Ni blades. The axial Ni atoms have identical coordination, although the La$_6$ prism around it is oriented along the *c* axis. La-Ni distances in the structure are in the range of 2.880–3.189(6) Å suggesting some charge transfer.

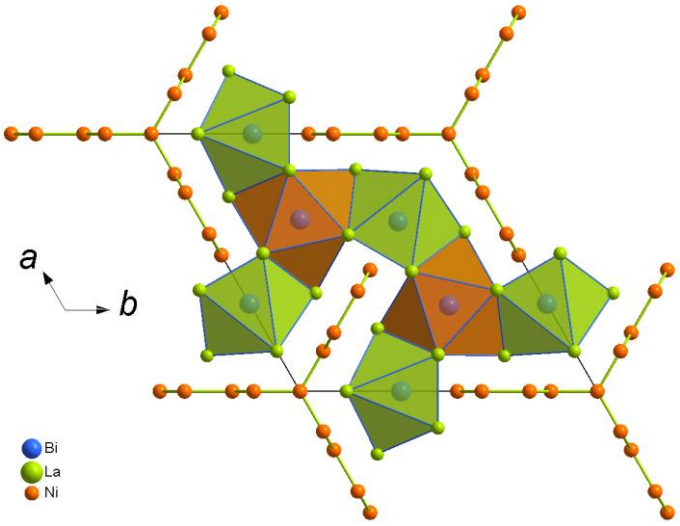

Figure 1. Projection of the crystal structure of $La_{15}Ni_{13}Bi_5$ along [001], with outlined Ni sticks and Bi polyhedra.

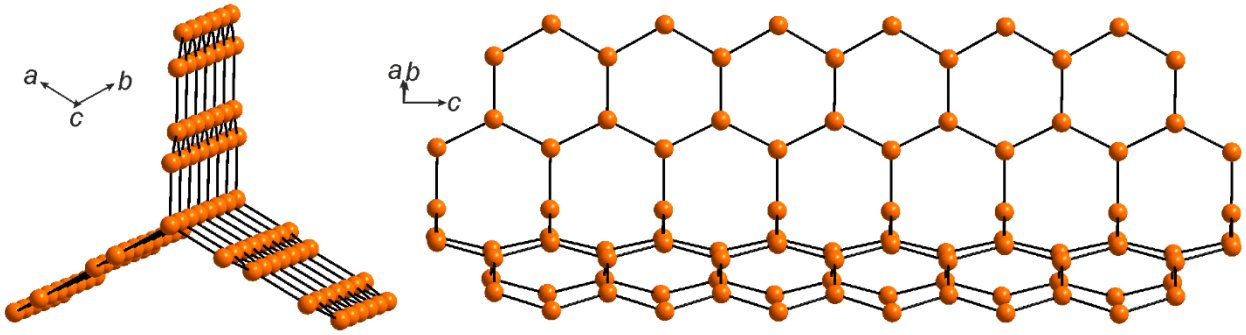

Figure 2. Ni stick in the crystal structure of $La_{15}Ni_{13}Bi_5$ extending along the *c* axis.

$La_9Ni_8Sn_5$ was detected during an attempt to explore possible isostructural representatives of $La_{15}Ni_{13}Bi_5$. No such compounds could be observed, though the discovered *p*-element-richer $La_9Ni_8Sn_5$ exhibits structural similarities, however with enhanced complexity partially due to extensive disorder. Contrary to $La_{15}Ni_{13}Bi_5$, $La_9Ni_8Sn_5$ is characterized by a polyanionic Ni/Sn network forming tunnels that encapsulate Sn-centered La polyhedra, $Sn@La_9$ (**Figure 3** and S6). They are constituted by a Sn-centered La_6 trigonal prism capped by three La atoms and remind of the $Bi@La_9$ polyhedra observed in $La_{15}Ni_{13}Bi_5$. The motif formed by Ni and Sn now extends in three directions though keeping the same basis – a three-blade turbine of Ni and Sn atoms (**Figure 4**). Further expansion beyond the Sn goes in two directions forming a nearly 90° angle between the branches (**Figure 4**, black arrows). Each of the branches is represented by Ni zigzag chains leading

to the row of Ni_4Sn_2 fused distorted hexagons. One of the chains is shared and responsible for connection with an identical basis leading to the formation of the framework. The other one goes towards the highly disordered area around the *c* axis. Interestingly, Ni-Ni distances in the basis are the shortest – 2.429(9) Å, while those in the zigzag chains are 2.616(4) Å due to geometric factors and higher influence of the competing interactions with the Sn atoms. Ni-Sn contacts in the ordered framework are in the ranges 2.723–2.789(5) Å.

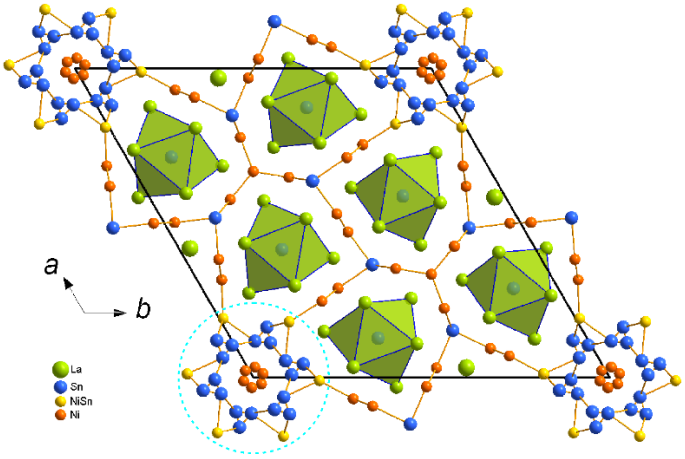

Figure 3. Projection of the crystal structure of $La_9Ni_8Sn_5$ along [001], with outlined Ni-Sn nets and Sn polyhedra. Sites within dashed blue circles are compositionally (Sn/Ni) or occupationally (Ln and Ni) disordered.

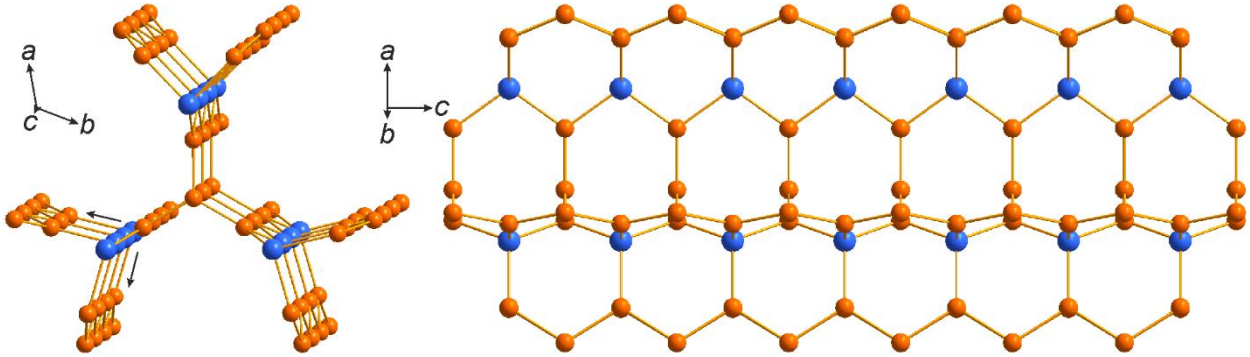

Figure 4. Ni-Sn framework in the crystal structure of $La_9Ni_8Sn_5$ extending along the *c* axis.

The area around the *c* axis is highly disordered (**Figure 3**, dashed circle), though that disorder can be rationalized. Such disorders occur mainly due to geometric reasons and are typical for hexagonal lanthanide compounds with transition and post-transition elements and a short *c*

axis.[43-45] Three sites are involved – the central Ni position is split over three locations with the total occupation of a hypothetical 2*a* position right on the *c* axis. The second layer includes heavily positionally disordered Sn 6*h* positions also split over three locations, while the last one is represented by mixed Ni/Sn occupation (0.67 Ni/0.33 Sn). Such composition assignment is confirmed by the results of EDX analysis, as well as interatomic distances to the neighboring Ni positions being in the upper range for the other observed Ni-Ni contacts in the structure and nearly equal to the sum of the corresponding covalent radii (2.58(1) Å).

As we mentioned before, $La_{15}Ni_{13}Bi_5$ has no direct analogies in the literature. Considering only the central part of the triangular motifs, geometrically similar fused hexagonal motifs could only be found in $La_{10}Co_7Ga_3$[46] though including also La atoms and offering no further expansion of the honeycomb network. Compositionally similar $Ce_{15}Ni_4Si_{13}$[47] exhibits a completely different packing, though, based on fused trigonal prismatic building blocks of the lanthanide atoms based on the ZrNiAl-type.[22] Indeed, $Ln_{(n+1)(n+2)}Ni_{n(n-1)+2}Si_{n(n+1)}$[43] exhibit features observed in both $La_{15}Ni_{13}Bi_5$ and $La_9Ni_8Sn_5$. Extensive positional disorder observed in $La_9Ni_8Sn_5$ is rather typical for related hexagonal structures, particularly those with a short *c* axis parameter.[47-50] While polyanionic tunnels with encapsulated cations are popular in intermetallics,[51] encapsulated mixed motifs are less common. For instance, complex mixed formations inside Au/In tunnels have been observed in Ca_3Au_3In.[52] Capped trigonal prismatic motifs both isolated and fused are quite common in binary intermetallics.[53-55]

3.2 Electronic structure

Previous investigations of the electronic structure of La-Ni-based compounds with additional *p*-elements, such as Sn, have shown that the occupied states of the valence band are mainly composed of flat 3*d*-Ni bands hybridized with 6*s*-La and 5*p*-Sn states, in which the 5*s*-Sn states are found at lower energy separated by a gap.[56]

The Density of States (DOS) of the present studied compounds, $La_{15}Ni_{13}Bi_5$ and $La_9Ni_8Sn_5$ are shown in **Figure 5a and 5b** respectively. When compared to the electronic structure of previously reported $LaNi_y$-based compounds,[56-57] that are rather Ni-rich, in the significantly La-richer compounds $La_{15}Ni_{13}Bi_5$ and $La_9Ni_8Sn_5$ significant electron transfer from La to Ni occurs as Bader charge analysis reveals, *c.f.* **Table 3**, with a Bader charge of about +1.2 electron for La. The localized, empty 4*f*-La states are located around 2 eV above the Fermi level. Thanks to the given

electrons from La, the 3*d*-Ni bands are almost entirely filled and a pseudo-gap arises at the Fermi level. Therefore, the DFT calculation converges in a Pauli paramagnetic state, even if ferromagnetic initialization is forced as a starting set.

The differences in the electronic structure of $La_{15}Ni_{13}Bi_5$ and $La_9Ni_8Sn_5$ is mainly due to different *p*-elements. Whereas the 6*s* band of Bi is found at -10 eV below Fermi level E_F, the 6*p*-Bi states interact well with La and Ni states in the range from -4 eV to E_F. Compared to that the 5*s* and 5*p* states of Sn are separated by a lower gap due to smaller scalar relativistic effects in Sn compared to Bi with a broader bonding 5*s* band of Sn located at about -8 eV featuring some interaction with Ni states, comparable to those found in compounds such as $LaNi_{4.75}Sn_{0.25}$.[56] The 5*p* states of Sn are located at higher energies interacting with the conduction *d*-metal bands, similar to those of 6*p*-Bi. Since bismuth is more electronegative than tin, it attracts more electrons: Bi and Sn present a Bader charge of 1.4 and 0.8 electrons respectively. The difference in electronic band dispersion, or here, energetic dispersion of the DOS, cannot only be attributed to the different energetic levels of the states but with respect to the *p*-states of the respective *p*-element, the ability to interact with its local environment, i.e. its next neighbors in the structure. In fact, in the case of $La_{15}Ni_{13}Bi_5$, Bi is isolated into La-prims whereas Sn is mixing with Ni in $La_9Ni_8Sn_5$. This is supported by the ELF plot as shown in **Figure 6**.

The ELF function exhibits maxima at the most probable positions of localized electron pairs and each maximum is surrounded by a basin (isosurface not shown) in which there is an increased probability of finding electrons. In fact, when high values for ELF are chosen, one can identify the electron pair domains that form the bonds. There is no maximum area between the atoms since there are no covalent bonds here. The system is characterized by metallic bonds with a rather low ELF and by the narrow width of the localization windows around atoms.[58] The last valence electron shell of La is missing due to the charge transfer. We can see that La contributes a smaller part of the bonding electrons than Ni and the *p*-element, as shown by the very localized pair-electron region located around the La and Bi/Sn atoms. The localized area of Sn is less important than that of Bi due to its interaction with Ni as discussed in the DOS analysis. Ni is surrounded by a non-localized electron region and forms a preferential metallic bond with other elements such as Sn, which supports the honeycomb framework. One can observe a localized region between some tin atoms resulting in a sparse Sn-Sn dumbbell appearance with one covalent bond, but this behavior

could not be generalized to all Sn-Sn bonds. In fact, it results from the random atoms distribution considered in the chosen periodic supercell, constrained by the partial occupation of the Sn1 site.

Both compounds are stable relative to the pure elements with a negative heat of formation of -54.00 and -47.23 kJ/mol for $La_{15}Ni_{13}Bi_5$ and $La_9Ni_8Sn_5$, respectively. Moreover, phonon calculation has been performed for the ordered $La_{15}Ni_{13}Bi_5$ structure. The phonon bands are shown in **Figure 7** with associated acoustic bands from heavier elements and optical flat bands associated with Ni elements around 6 THz. The vibrational dispersion curves present no imaginary frequency yielding the confirmation of the mechanical stability of the honeycomb network in the $La_{15}Ni_{13}Bi_5$ phase.

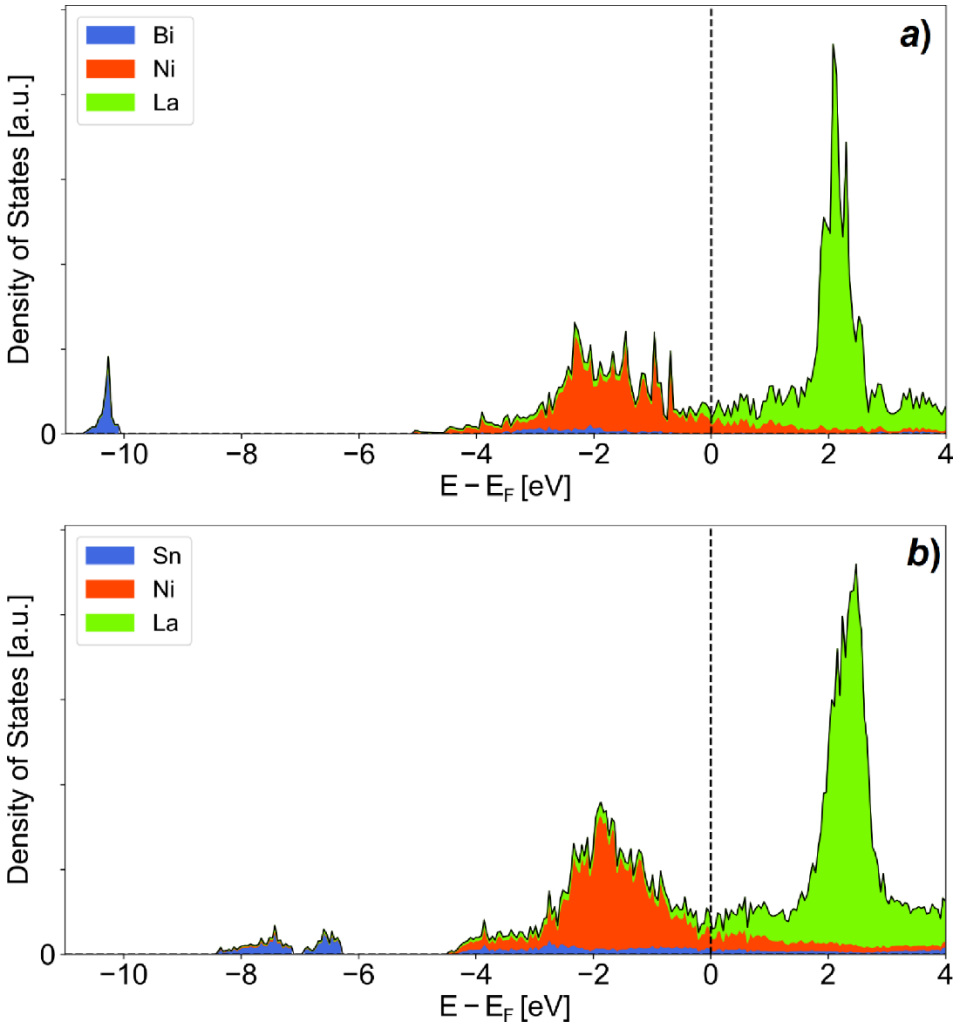

Figure 5. The total density of state (black line) with site-projected contributions of all atoms in $La_{15}Ni_{13}Bi_5$ (a) and $La_9Ni_8Sn_5$ (b). Fermi level is chosen as the origin of the energy.

Table 3. Average Bader electronic charge by atom, for $La_{15}Ni_{13}Bi_5$ and $La_9Ni_8Sn_5$.

Atom / Compound	La	Ni	Bi / Sn
$La_{15}Ni_{13}Bi_5$	- 1.18	+ 0.82	+ 1.41
$La_9Ni_8Sn_5$	- 1.16	+ 0.80	+ 0.80

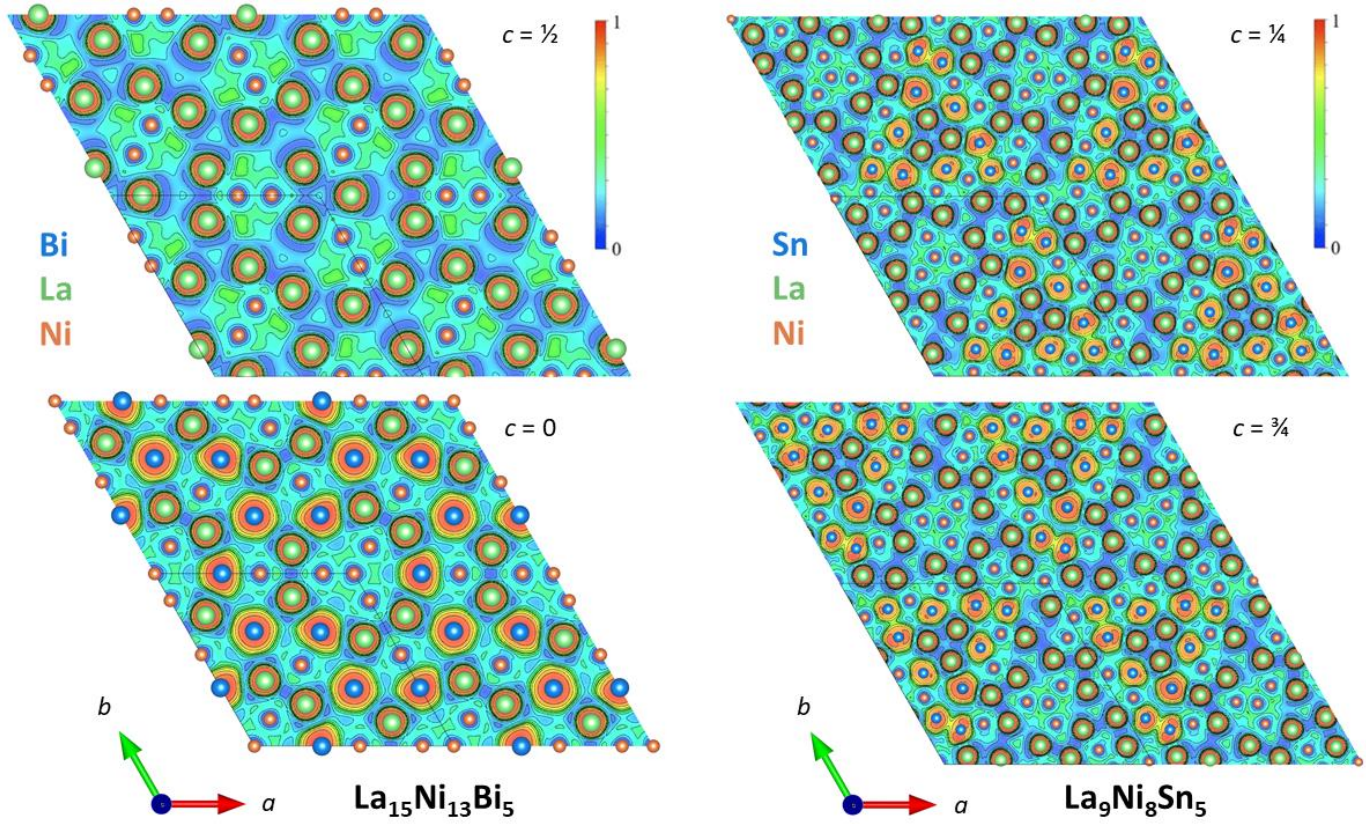

Figure 6. ELF representation of $La_{15}Ni_{13}Bi_5$ and an ordered approximation of $La_9Ni_8Sn_5$ at two different plans perpendicular to the *c* axis. Warm color (red) areas indicate a strongly localized pair-electrons zone (probability of presence close to 1), whereas cold color (blue) represents nonlocalized electrons.

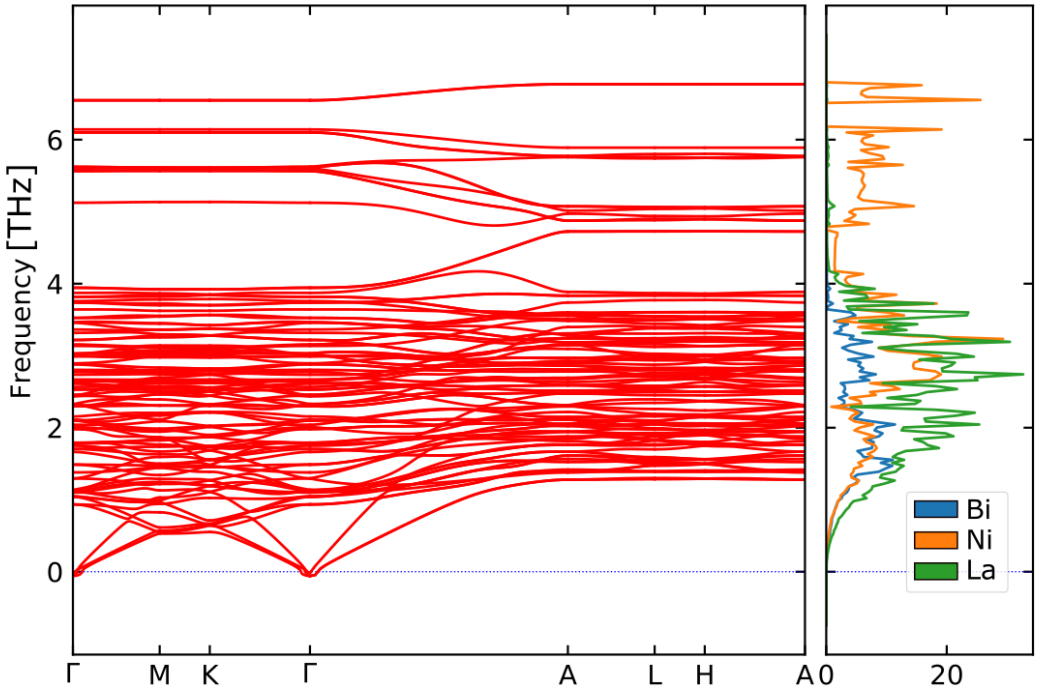

Figure 7. Phonon dispersion curves for $La_{15}Ni_{13}Bi_5$.

3.3 Magnetic behavior

The results from magnetic measurements for $La_9Ni_8Sn_5$ are presented in **Figure 8**. The magnetic susceptibility at 100 Oe shows a complex behavior with a plateau between 50-100 K, while at lower temperatures both FC and ZFC curves go to lower values. For higher fields the above behavior is suppressed, being a mark of weak magnetism. Inverse magnetization does not follow the Curie-Weiss law (even the modified) for fields less than 1 kOe. Applying a high magnetic field partially linearize the inverse magnetic susceptibility, as presented in **Figure S7** (SI). Extraction of ferromagnetic impurity by the Honda-Owen method also does not show results that can be easily interpreted (**Figure S7**). Therefore, it may be concluded that the magnetic properties of the compound are presumably weakly- or para-magnetic, overlayed on magnetism originating from spurious phases. According to our XRD/EDX studies, small amounts of impurities were detected (see **Figures S1 and S2** in SI). Eg. the La_2Ni_7 is an itinerant weak antiferromagnet with an ordering temperature of 51 K (wAFM).[59] $LaNi_3$ was detected as the other impurity. According to the literature, it shows weak itinerant magnetism below 28 K, while neutron diffraction showed no magnetic contribution, at all.[60] Additionally, EDX results indicated

extremely small precipitations of Ce (cerium is a common impurity encountered in La, even in commercial 99.9% La). As Ce shows complex magnetic ordering at 12.5 K, the upturn of susceptibility could be associated with Ce precipitations. Small ferromagnetic components visible for all isothermal magnetization curves are presumably related to small amounts of Ni precipitations. However, it is worth mentioning that no exchange bias was noticed for the curves, which may originate in the nanostructural morphology of the Ni precipitations. It is also evident that the shape of FC/ZFC curves, with broad anomaly, resembles behavior often seen for low-dimensional magnets.[61]

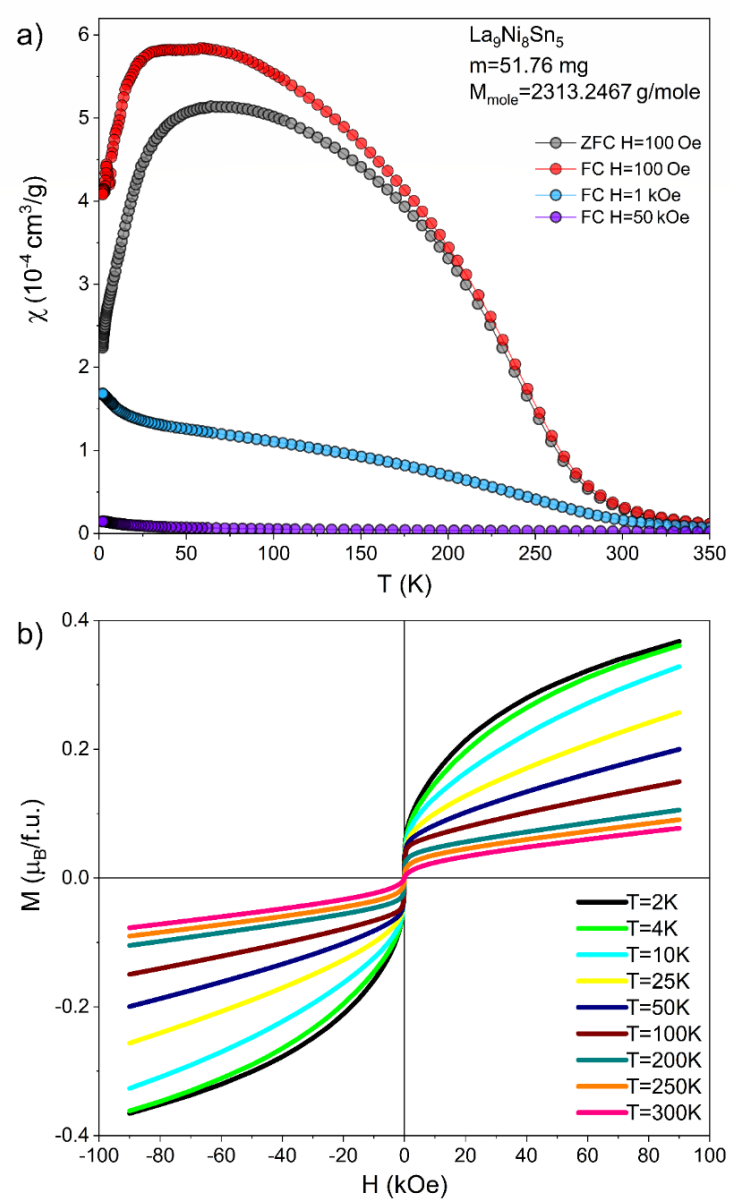

Figure 8. Magnetic properties of $La_9Ni_8Sn_5$: susceptibility measured at different magnetic fields (a) and isothermal magnetization (b).

For the $La_{15}Ni_{13}Bi_5$ compound, magnetic susceptibility *vs*. temperature is shown in **Figure 9**. As apparent, in the 25-300K temperature range, the magnetic susceptibility is dominated by small ferromagnetic components. It can be seen in the insert to **Figure 9**, where isothermal magnetization curves show a ferromagnetic component between 2-300K. The ferromagnetic component most likely originates from very small Ni-rich precipitates (due to alloy decomposition/oxidation on air during the preparation of the sample for magnetic measurement). Interestingly, at low temperatures, below 10 K ZFC and FC curves show some anomalous behavior. This presumably originates from $La_{1-x}Ce_xBi$ (CeBi and pure Ce impurities, which order magnetically at 26 K and 12.5 K, respectively).[62-63]

Inverse magnetic susceptibility measured at high magnetic fields (50 kOe) did not show Curie-Weiss behavior, therefore, estimating the effective magnetic moment was not possible. Nonetheless, a broad maximum in the ZFC curve suggests some dimensionally-restricted magnetism.

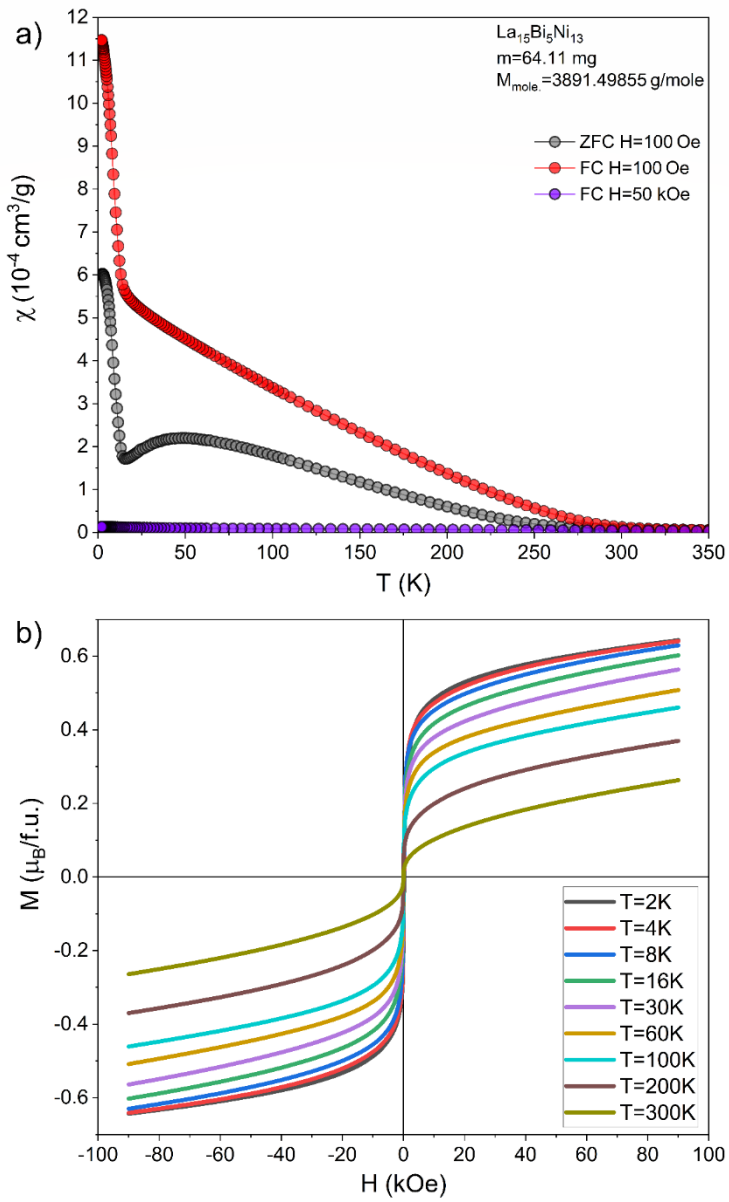

Figure 9. Magnetic properties of $La_{15}Ni_{13}Bi_5$: susceptibility measured at different magnetic fields (a) and isothermal magnetization (b).

4. Conclusion

The new ternary intermetallics $La_{15}Ni_{13}Bi_5$ and $La_9Ni_8Sn_5$ have been synthesized and their properties investigated. The crystal structure of $La_{15}Ni_{13}Bi_5$ is characterized by pseudo-1D honeycomb-based motifs of Ni atoms surrounded by La atoms. $La_9Ni_8Sn_5$ contrary is characterized by a honeycomb-based polyanionic Ni/Sn network encapsulating Sn-centered polyhedra. The latter

structure exhibits substantial disorder in the area around the *c* axis. Honeycomb-based motifs observed in both compounds extend along the *c* axis in contrast to planar or pseudoplanar layers in graphite or similar inorganic structures where such constructs are normal to the 3(6)-fold axis. The core building fragments of the honeycomb motifs bear some analogies to organic aromatic molecules like triptycene while the pseudo-1D construct observed in $La_{15}Ni_{13}Bi_5$ is, to the best of our knowledge, unique in the solid state.

Magnetometric measurements revealed that $La_9Ni_8Sn_5$ is likely exhibiting paramagnetism or weak magnetism with magnetic response dominated by spurious La-Ni phases. On the other hand, $La_{15}Ni_{13}Bi_5$ is probably a Pauli paramagnet with magnetic properties biased by ferromagnetic impurities; however, some sigh of low dimensional magnetism could be noticed in the ZFC curve.

DFT and phonon calculations confirm the mechanical stability of these honeycomb constructs explained by a metallic bond with an electronic charge transfer from La to Ni and the Bi/Sn atoms.

ASSOCIATED CONTENT

Supporting information

The Supporting Information is available free of charge at https://pubs.acs.org/doi/10.1021/. Additional crystallographic information, **Figures S1-S7**.

Accession Codes

CCDC 2241021 and 2241022 contain supplementary crystallographic data for this paper. These data can be obtained free of charge via www.ccdc.cam.ac.uk/data_request/cif, or by emailing data_request@ccdc.cam.ac.uk, or by contacting The Cambridge Crystallographic Data Centre, 12 Union Road, Cambridge CB2 1EZ, UK; fax: +44 1223 336033.

AUTHOR INFORMATION

Corresponding Authors

Vitalii Shtender – Department of Chemistry – Ångström Laboratory, Uppsala University, Box 538, 75121 Uppsala, Sweden; orcid.org/0000-0002-8690-9957; Email: vitalii.shtender@kemi.uu.se

Authors

Volodymyr Smetana – Department of Materials and Environmental Chemistry, Stockholm University, 10691 Stockholm, Sweden; orcid.org/0000-0003-0763-1457

Jean-Claude Crivello – Univ Paris Est Creteil, CNRS, ICMPE, UMR7182, 2 rue Henri Dunant, 94320 Thiais, France; orcid.org/0000-0002-4849-2556

Łukasz Gondek – AGH University of Science and Technology, Faculty of Physics and Applied Computer Science, Mickiewicza 30, 30-059, Krakow, Poland; orcid.org/0000-0002-4149-7944

Janusz Przewoźnik – AGH University of Science and Technology, Faculty of Physics and Applied Computer Science, Mickiewicza 30, 30-059, Krakow, Poland; orcid.org/0000-0002-2313-7611

Anja-Verena Mudring – Department of Materials and Environmental Chemistry, Stockholm University, 10691 Stockholm, Sweden; orcid.org/0000-0002-2800-1684

Martin Sahlberg – Department of Chemistry – Ångström Laboratory, Uppsala University, Box 538, 75121 Uppsala, Sweden

Author contributions

The manuscript was written through the contributions of all authors. All authors have approved the final version of the manuscript.

Notes

The authors declare no competing financial interest.

ACKNOWLEDGMENTS

We acknowledge Myfab Uppsala for providing facilities. Myfab is funded by the Swedish Research Council as a national research infrastructure. Financial support from the Foundation for Strategic Research (SSF), grant #EM16-0039, as well as from ÅForsk is gratefully acknowledged. DFT calculations were performed using HPC resources from GENCI–CINES (Grant A0060906175).

References

1. *Bismuth-Containing Compounds*. Springer New York, NY, 2013.
2. Mar, A., In *Handbook on the Physics and Chemistry of Rare Earths vol. 36*, Gschneider Jr., K. A.; Bünzli, J.-C. G.; Pecharsky, V. K., Eds. Elsevier B.V.: North Holland, 2006; pp 1– 82.
3. Pöttgen, R., Stannides and Intermetallic Tin Compounds – Fundamentals and Applications. *Z. Naturforsch. B* **2006,** *61* (6), 677-698, 10.1515/znb-2006-0607.
4. Matthias, B. T.; Geballe, T. H.; Compton, V. B., Superconductivity. *Reviews of Modern Physics* **1963,** *35* (1), 1-22, 10.1103/RevModPhys.35.1.
5. Weitzer, F.; Hiebl, K.; Rogl, P., Crystal chemistry and magnetism of neodymium stannides including compounds of the structural series RE_nSn_{3n-2}. *J. Solid State Chem.* **1992,** *98* (2), 291-300, 10.1016/S0022-4596(05)80237-3.
6. Singh, S.; Kumar, R., Superconducting Properties of $LaSn_3$ Under Positive Hydrostatic Pressure. *J. Supercond. Nov. Magn.* **2019,** *32* (11), 3431-3436, 10.1007/s10948-019-5134-0.
7. Buta, F.; Bonura, M.; Matera, D.; Bovone, G.; Ballarino, A.; Hopkins, S. C.; Bordini, B.; Chaud, X.; Senatore, C., Very high upper critical fields and enhanced critical current densities in Nb_3Sn superconductors based on Nb–Ta–Zr alloys and internal oxidation. *Journal of Physics: Materials* **2021,** *4* (2), 025003, 10.1088/2515-7639/abe662.
8. Sun, D.; Wang, Y.; Livi, K. J. T.; Wang, C.; Luo, R.; Zhang, Z.; Alghamdi, H.; Li, C.; An, F.; Gaskey, B.; Mueller, T.; Hall, A. S., Ordered Intermetallic Pd_3Bi Prepared by an Electrochemically Induced Phase Transformation for Oxygen Reduction Electrocatalysis. *ACS Nano* **2019,** *13* (9), 10818-10825, 10.1021/acsnano.9b06019.
9. Bismuth, Bismuth Alloys, and Bismuth Compounds. In *Ullmann's Encyclopedia of Industrial Chemistry*, Krüger, J.; Winkler, P.; Lüderitz, E.; Lück, M.; Wolf, H. U., Eds. John Wiley & Sons, Ltd 2003.
10. Bigun, I.; Smetana, V.; Mudryk, Y.; Hlova, I.; Dzevenko, M.; Havela, L.; Kalychak, Y.; Pecharsky, V.; Mudring, A.-V., $EuNi_5InH_{1.5-x}$ (x = 0–1.5): hydrogen induced structural and magnetic transitions. *J. Mater. Chem. C* **2017,** *5* (12), 2994-3006, 10.1039/C7TC00121E.
11. Sato, M.; Yartys, V. A., Hydrogen absorption–desorption characteristics of the $LaNi_5Sn$ intermetallic compound. *J. Alloys Compd.* **2004,** *373* (1), 161-166, 10.1016/j.jallcom.2003.10.027.
12. Zhuang, Y.; Deng, H.; Liu, J.; Yao, Q., The 673 K isothermal section of the La–Ni–Sn ternary system. *J. Alloys Compd.* **2004,** *363* (1), 228-231, 10.1016/S0925-8388(03)00475-4.
13. Skolozdra, R. V.; Komarovskaya, L. P. Crystal structure and magnetic susceptibility of RNi5Sn compounds, Dopovidi Akademii Nauk Ukrains'koi RSR, Seriya A: Fiziko-Matematichni ta Tekhnichni Nauki, Dopov. Akad. Nauk Ukr. RSR, Ser. A (1982), 6, 80-82.
14. Skolozdra, R. V.; Yasnitskaya, I. V.; Akselrud, L. G.; Komarovskaya, L. P., Structure and properties of RNi4Sn2, R= La, Ce, Pr, Nd, or Sm. *Neorg. Mater.* **1988,** *24*, 69-72.
15. Kaczmarska, K.; Pierre, J.; Slebarski, A.; Skolozdra, R. V., Magnetic properties and resistivity of CeM_2X_2 compounds (M = Cu, Ni; X = Sn, Sb). *J. Alloys Compd.* **1993,** *196* (1), 165-170, 10.1016/0925-8388(93)90589-F.
16. Dörrscheidt, W.; Savelsberg, G.; Stöhr, J.; Schäfer, H., Beiträge zu den stabilitätskriterien der $BaCuSn_2$-struktur: Die verbindungen $LaCu_{0,56}Sn_2$, $LaNi_{0,74}Sn_2$, $LaCo_{0,52}Sn_2$, $LaFe_{0,34}Sn_2$ und $BaCuSn_2$. *J. Less Common Met.* **1982,** *83* (2), 269-278, 10.1016/0022-5088(82)90277-6.
17. Skolozdra, R. V.; Yasnitskaya, I. V.; Akselrud, L. G., Properties of new stannides of rare-earth metals with the structure type $La_3Co_2Sn_7$. *Ukr. Phys. J.* **1987,** *32*, 729-732.

18. Komarovska, L. P.; Skolozdra, R. V., New GdNi2.67Sn5.44 structural type representatives and their magnetic properties. *Dopovidi Akademii Nauk Ukrains'koi RSR, Seriya A: Fiziko-Matematichni ta Tekhnichni Nauki* **1985,** *47*, 78-80.
19. Dwight, A. E., Crystal structure of RENiSn and REPdsn (RE = rare earth) equiatomic compounds. *J. Less Common Met.* **1983,** *93* (2), 411-413, 10.1016/0022-5088(83)90195-9.
20. Nakamura, Y.; Bowman, R. C.; Akiba, E., Strain formation and lattice parameter change in $LaNi_{4.75}Sn_{0.25}$–H system during the initial activation process. *J. Alloys Compd.* **2004,** *373* (1), 183-193, 10.1016/j.jallcom.2003.10.049.
21. Zhuang, Y. H.; Deng, H. X.; Liu, J. Q.; Yao, Q. R., The 673 K isothermal section of the La-Ni-Sn ternary system. *J. Alloys Compd.* **2004,** *363* (1-2), 223-226, 10.1016/S0925-8388(03)00475-4.
22. Heymann, G.; Heying, B.; Rodewald, U. C.; Janka, O.; Huppertz, H.; Pöttgen, R., High-pressure high-temperature crystal growth of equiatomic rare earth stannides RENiSn and REPdSn. *J. Solid State Chem.* **2016,** *236*, 138-146, 10.1016/j.jssc.2015.06.044.
23. Ott, C.; Baumgartner, M.; Schäfer, K.; Baumer, F.; Freitag, K.; Scherf, L.; Heletta, L.; Weihrich, R.; Pöttgen, R.; Nilges, T., Structure and Bonding of La_2NiBi. *Z. Anorg. Allg. Chem.* **2019,** *645* (3), 340-346, 10.1002/zaac.201800237.
24. Hofmann, W. K.; Jeitschko, W., Ternary pnictides $MNi_{2-x}Pn_2$ (M ≡ Sr and rare earth metals, Pn ≡ Sb, Bi) with defect $CaBe_2Ge_2$ and defect $ThCr_2Si_2$ structures. *J. Less Common Met.* **1988,** *138* (2), 313-322, 10.1016/0022-5088(88)90119-1.
25. Lin, X.; Straszheim, W. E.; Bud'ko, S. L.; Canfield, P. C., Anisotropic magnetization and resistivity of single crystalline $RNi_{1-x}Bi_{2\pm y}$ (R=La–Nd, Sm, Gd–Dy). *J. Alloys Compd.* **2013,** *554*, 304-311, 10.1016/j.jallcom.2012.11.138.
26. Haase, M. G.; Jeitschko, W. Ternary Lanthanoid Transition Metal Bismuthides and Related Compounds with TiNiSi, ZrNiAl, MgAgAs, $Y_3Au_3Sb_4$, and Mo_5Si_3C Type Structures, Thirteenth International Conference on Solid Compounds of Transition Elements, Stresa, Italy, Collected Abstracts$Abstr. 13th Int. Conf. Solid Compd. Transition Elem. (2000), P-B09.
27. Kraus, W.; Nolze, G., POWDER CELL - A program for the representation and manipulation of crystal structures and calculation of the resulting X-ray powder patterns. *J. Appl. Crystallogr.* **1996,** *29*, 301-303, 10.1107/S0021889895014920.
28. *APEX3 and SAINT. Bruker AXS Inc., Madison, Wisconsin, USA.*, 2015.
29. Krause, L.; Herbst-Irmer, R.; Stalke, D., An empirical correction for the influence of low-energy contamination. *J. Appl. Crystallogr.* **2015,** *48* (6), 1907-1913, 10.1107/S1600576715020440.
30. Sheldrick, G., SHELXT - Integrated space-group and crystal-structure determination. *Acta Crystallogr. Sect. A* **2015,** *71* (1), 3-8, 10.1107/S2053273314026370.
31. Sheldrick, G., Crystal structure refinement with SHELXL. *Acta Crystallogr. Sect. C: Struct. Chem.* **2015,** *71* (1), 3-8, 10.1107/S2053229614024218.
32. Kresse, G.; Joubert, D., From ultrasoft pseudopotentials to the projector augmented-wave method. *Phys. Rev. B* **1999,** *59* (3), 1758-1775.
33. Kresse, G.; Furthmüller, J., Efficient iterative schemes for ab initio total-energy calculations using a plane-wave basis set. *Phys. Rev. B* **1996,** *54* (16), 11169-11186.
34. Perdew, J. P.; Burke, K.; Ernzerhof, M., Generalized gradient approximation made simple *Phys. Rev. Lett.* **1997,** *78* (7), 1396-1396, 10.1103/PhysRevLett.78.1396.
35. Parlinski, K.; Li, Z. Q.; Kawazoe, Y., First-principles determination of the soft mode in cubic ZrO_2. *Phys. Rev. Lett.* **1997,** *78* (21), 4063-4066, 10.1103/PhysRevLett.78.4063.

36. Togo, A.; Oba, F.; Tanaka, I., First-principles calculations of the ferroelastic transition between rutile-type and $CaCl_2$-type SiO_2 at high pressures. *Phys. Rev. B* **2008,** *78* (13), ARTN 134106

10.1103/PhysRevB.78.134106.
37. Grin, Y.; Savin, A.; Silvi, B., *The ELF perspective of chemical bonding, The chemical bond*. 2014.
38. Wagner, F. R.; Grin, Y., 3.09 - Chemical bonding analysis in position space. In *Comprehensive Inorganic Chemistry III (Third Edition)*, Reedijk, J.; Poeppelmeier, K. R., Eds. Elsevier: Oxford, 2023; pp 222-237.
39. Van der Maelen, J. F., Topological Analysis of the Electron Density in the Carbonyl Complexes $M(CO)_8$ (M = Ca, Sr, Ba). *Organometallics* **2020,** *39* (1), 132-141, 10.1021/acs.organomet.9b00699.
40. Momma, K.; Izumi, F., VESTA 3 for three-dimensional visualization of crystal, volumetric and morphology data. *J. Appl. Crystallogr.* **2011,** *44*, 1272-1276, 10.1107/S0021889811038970.
41. Henkelman, G.; Arnaldsson, A.; Jonsson, H., A fast and robust algorithm for Bader decomposition of charge density. *Comput. Mater. Sci.* **2006,** *36* (3), 354-360, 10.1016/j.commatsci.2005.04.010.
42. Cordero, B.; Gomez, V.; Platero-Prats, A. E.; Reves, M.; Echeverria, J.; Cremades, E.; Barragan, F.; Alvarez, S., Covalent radii revisited. *Dalton Trans.* **2008,** (21), 2832-2838, 10.1039/B801115J.
43. Prots, Y. M.; Jeitschko, W., Lanthanum Nickel Silicides with the General Formula $La_{(n+1)(n+2)}Ni_{n(n-1)+2}Si_{n(n+1)}$ and Other Series of Hexagonal Structures with Metal:Metalloid Ratios Close to 2:1. *Inorg. Chem.* **1998,** *37* (21), 5431-5438, 10.1021/ic980397w.
44. Pivan, J. Y.; Guerin, R.; Sergent, M., A new classification scheme to describe and predict structure types in pnictide and silicide chemistry. *J. Solid State Chem.* **1987,** *68*, 11-21.
45. Grilli, D.; Smetana, V.; Ahmed, S.; Shtender, V.; Pani, M.; Manfrinetti, P.; Mudring , A.-V., $La_{n(n+1)+x}Ni_{n(n+5)+y}Si_{(n+1)(n+2)-z}$: A Symmetric Mirror Homologous Series in the La-Ni-Si System. *Inorg. Chem.* **2023,** *62*, 10736-10742, 10.1021/acs.inorgchem.3c01194.
46. Grin', Y.; Yarmolyuk, Y. P.; Gladyshevskii, E. I., Crystal structure of compounds $R_{10}Ga_3Co_7$ (R = Y, La). *Kristallografiya* **1979,** *24* (3), 455-460.
47. Gladyshevskii, E. I.; P.I., K., Homologous series including the new structure types of ternary silicides. *Acta Crystallogr. Sect. A* **1972,** *28*, S97a.
48. Kotur, B.; Babizhetskyy, V.; Smetana, V.; Zheng, C.; Mudring, A. V., Crystal and electronic structures of the new ternary silicide $Sc_{12}Co_{41.8}Si_{30.2}$. *J. Solid State Chem.* **2021,** *302*, 122373, 10.1016/j.jssc.2021.122373.
49. Smetana, V.; Miller, G. J.; Corbett, J. D., Three Alkali-Metal–Gold–Gallium Systems. Ternary Tunnel Structures and Some Problems with Poorly Ordered Cations. *Inorg. Chem.* **2012,** *51* (14), 7711-7721, 10.1021/ic300740u.
50. Smetana, V.; Miller, G. J.; Corbett, J. D., Polyclusters and Substitution Effects in the Na–Au–Ga System: Remarkable Sodium Bonding Characteristics in Polar Intermetallics. *Inorg. Chem.* **2013,** *52* (21), 12502-12510, 10.1021/ic401580y.
51. Smetana, V.; Rhodehouse, M.; Meyer, G.; Mudring, A.-V., Gold polar intermetallics: structural versatility through exclusive bonding motifs. *Acc. Chem. Res.* **2017,** *50* (11), 2633-2641, 10.1021/acs.accounts.7b00316.

52. Muts, I. R.; Zaremba, V. I.; Rodewald, U. C.; Pöttgen, R., Infinite Gold Zig-Zag Chains as Structural Motif in Ca_3Au_3In – A Ternary Ordered Variant of the Ni_4B_3 Type. *Z. Anorg. Allg. Chem.* **2008,** *634* (1), 56-60, 10.1002/zaac.200700305.
53. Ovchinnikov, A.; Mudring, A.-V., Overlooked Binary Compounds Uncovered in the Reinspection of the La–Au System: Synthesis, Crystal Structures, and Electronic Properties of La_7Au_3, La_3Au_2, and La_3Au_4. *Inorg. Chem.* **2021,** *60* (16), 12158-12171, 10.1021/acs.inorgchem.1c01355.
54. Bell, T.; Celania, C. R.; Smetana, V.; Mudring, A.-V.; Meyer, G., Tb_3Pd_2, Er_3Pd_2 and Er_6Co_{5-x}: structural variations and bonding in rare-earth-richer binary intermetallics. *Acta Crystallogr. C* **2018,** *74* (9), 991-996, 10.1107/S2053229618010549.
55. Rhodehouse, M. L.; Bell, T.; Smetana, V.; Mudring, A.-V.; Meyer, G. H., An Obscured or Nonexistent Binary Intermetallic, Co_7Pr_{17}, Its Existent Neighbor Co_2Pr_5, and Two New Ternaries in the System Co/Sn/Pr, $CoSn_3Pr_{1-x}$, and $Co_{2-x}Sn_7Pr_3$. *Cryst. Growth Des.* **2018,** *18* (10), 6273-6283, 10.1021/acs.cgd.8b01141.
56. Crivello, J. C.; Gupta, M., Electronic properties of $LaNi_{4.75}Sn_{0.25}$, $LaNi_{4.5}M_{0.5}$ (*M*= Si, Ge, Sn), $LaNi_{4.5}Sn_{0.5}H_5$. *J. Alloys Compd.* **2003,** *356*, 151-155, 10.1016/S0925-8388(02)01224-0.
57. Crivello, J. C.; Zhang, J.; Latroche, M., Structural Stability of AB_y Phases in the (La,Mg)-Ni System Obtained by Density Functional Theory Calculations. *J Phys Chem C* **2011,** *115* (51), 25470-25478, 10.1021/jp204835z.
58. Silvi, B.; Gillespie, R.; Gatti, C., Electron Density Analysis. *Comprehensive Inorg. Chem. II* **2013,** *9*, 187-226, 10.1016/B978-0-08-097774-4.00907-4.
59. Ribeiro, R. A.; Bud'ko, S. L.; Xiang, L.; Ryan, D. H.; Canfield, P. C., Small-moment antiferromagnetic ordering in single-crystalline La_2Ni_7. *Phys. Rev. B* **2022,** *105* (1), 014412, 10.1103/PhysRevB.105.014412.
60. Tazuke, Y.; Abe, M.; Funahashi, S., Magnetic properties of La-Ni system. *Physica B* **1997,** *237*, 559-560, 10.1016/S0921-4526(97)00245-7.
61. Vasil'ev, A. N.; Markina, M. M.; Popova, E. A., Spin gap in low-dimensional magnets (Review). *Low Temperature Physics* **2005,** *31* (3), 203-223, 10.1063/1.1884423.
62. Grimberg, A. J. T.; Schinkel, C. J.; Zandee, A. P. L. M., The magnetic and electrical properties of pure α-cerium at atmospheric pressure. *Solid State Commun.* **1972,** *11* (11), 1579-1583, 10.1016/0038-1098(72)90523-6.
63. Nereson, N.; Arnold, G., Magnetic Properties of CeBi, NdBi, TbBi, and DyBi. *J. Appl. Phys.* **1971,** *42* (4), 1625-1627, 10.1063/1.1660369.